scientific reports

Check for updates

OPEN

DFT study to discover new EIL materials based on the quinolate derivatives involving S and Se atoms

Sunwoo Kang[1]✉ & Taekyung Kim[2]✉

We designed a series of new EIL molecules based on the Liq. As a simple design strategy, S and Se atoms were utilized to replace O atom of quinolate moiety. Additionally, the quinolate derivatives including S and Se atoms with singly oxidized metal ions (Na^+, K^+, Rb^+, Cs^+, Ag^+, and Au^+) were also designed. The DFT and TDDFT calculations were performed to understand the charge transport, and photophysical properties of designed molecules. As a result, the AuSq and AuSeq are expected to provide benefits to develop the OLED device performance. First, faster electron hopping rate and lower injection barrier are expected to increase the amount of electron carriers into EML, which crucially helps to improve the exciton recombination rate and *J-V* characteristic. Eventually, the external quantum efficiency and power efficiency are expected to increase. Moreover, these designed molecules hardly absorb any primary colors, thereby they don't reduce the out-coupled light photons. Based on these results, we strongly suggest that AuSq and AuSeq can be utilized as alternative EIL material to achieve the superior performance in OLED devices.

Keywords Density functional theory simulation, Charge transport property, ETL-Liq complex, Absorption property

Since the first report by Tang and Van Slyke[1] the organic light emitting-diode (OLED) technology has been greatly developed and become a huge mainstream in the display industry since its excellent merits for color purity, wide view angle, contrast, flexibility, and brightness takes remarkable advantages to manufacture of the electronic devices, which are closely related to our daily life[2–5]. In the early stage, the device architecture of OLED has basically consisted of three organic layers, known as hole transport layer, electron transport layer, and emissive layer. However, the simple device architecture cannot meet the minimal criteria of the required efficiency and durability to commercialize in the display industry. To overcome the critical issue, much effort had been attempted to improve the efficiency and durability in terms of developing the material properties and evolving the device architecture[6–17]. In the point of device architecture view, it is worthying noticed from the device architecture that the hole/electron injection layer (HIL/EIL) and hole/electron buffer layers (BL) were additionally adopted to mainly manipulate the balance of the hole/electron carriers and suppression of the hole/electron leakage. In addition, the pivotal materials properties such as mobility, photoluminescent quantum yield (PLQY), and internal quantum efficiency (IQE) were intensely studied to achieve the meet of the commercial standardization of efficiency and durability in the display industry. Since then, the tremendous endeavors to engineer the new organic/organometallic materials for HIL, HTL, ETL, EML, and BL have been intensely investigated and reported until now. However, designing a new material based on lithium-quinolin-8-olate (Liq)[18] known as EIL, is rarely investigated and reported. In the industry and academy, Liq is typically co-deposited with ETM to manipulate the amount of electron carrier. The role of Liq is to manipulate the amount of electron carriers in terms of the injection and transport. In detail, the LUMO energy level of Liq, which is closely aligned with the work-function of cathode, aids the spontaneous injection of the electron to increase the probability of exciton recombination in EML. Moreover, the slow electron mobility of Liq plays a key role in mitigating the significant activation of the exciton-polaron quenching. Therefore, Liq is understood as a one of important components in influencing the efficiency and lifetime of OLED device. In this perspective, we assure that searching the new materials modified from Liq is also required to contribute to the enhancement

[1]Department of Chemistry, Dankook University, Cheonan 448- 701, Chungnam, Republic of Korea. [2]Department of Chemical Engineering, Kyung Hee University, Yongin-si 17104, Republic of Korea. ✉email: sunwoo.kang@dankook.ac.kr; taekyung.kim@khu.ac.kr

of the efficiency and lifetime in OLED device. Basically, the structural feature of Liq is that the Li^+ interacts with the O^- and N atoms through the ionic and coordination bonding. Based on the molecular structure of Liq, the easiest design strategy is to replace the Li^+ by other singly oxidized metal ions (M^+). On the basis of mentioned strategy, we previously investigated the effect of different M^+ on the electronic and charge transport properties of M^+-quinolin-8-olate (Mq) and M^{2+}-(quinolin-8-olate)$_2$ (Mq_2) through the density functional theory (DFT) calculation[19,20]. In addition, there are several attempts to modify quinolate moiety of Liq. For example, the lithium 2-methyl 8-hydroxyquiolinate (MeLiq) and lithium 2-phenyl 8-hydroxyquinoliate (PhLiq) were synthesized to understand the steric bulk effect on the aggregation behavior[21]. In 2008, the theoretical study for CN-substituted Liq (5-CN-Liq) was reported to gain the insight of the role of CN substituent on electronic and photophysical properties[22]. Despite the considering the previous reports, there is still unexplored design space in quinoline-8-olate, where the O atom can be replaced by S and Se atoms. In addition to this, the effect of the M^+ ions on the quinoline-8-thiolate (Sq^-) and quinoline-8-selenolate (Seq^-) should be further studied to revisit the role the different M^+ ion on the electronic and charge transport properties in M^+-Sq^- (MSq) and M^+-Seq^- (MSeq) complexes. Similar to the previous report[20]Na^+, K^+, Rb^+, Cs^+, Ag^+, and Au^+ ions were representatively chosen as M^+.

In this study, we mainly investigated the electronic and charge transport properties of M^+-QS^- and M^+-QSe^- complexes. Moreover, the complexation behavior with ETL and absorption properties were considered to understand the disadvantageous effect on the charge transport and outcoupling efficiency for primary colors in the OLED device. To the best of our knowledge, we expect that this study will help to extend the design space as well as to gain the pivotal insight for finding new EIL materials.

Theory and computation

Density functional theory (DFT) calculations were carried out by employing a non-local density functional of Becke's three parameterized Lee-Yang-Parr exchange functional (B3LYP)[23–25] with Pople's triple zeta potential with double polarization function (6-311G**) for C, H, N, O, S, Se, Na, and K atoms and a Hay-Watt effective core potential (LANL2DZ) for Rb, Cs, Ag, and Au atoms, as implemented in the suite of Gaussian 16 program[26]. All molecular structures in neutral, cation, and anion state were fully optimized without symmetry constrains and their thermodynamic stabilities were verified by frequency calculations. According to the Marcus electron transfer theory[27] the charge transport properties have been known to be critically influenced by reorganization energy (λ_h or λ_e) and transfer integral (t_h or t_e). In detail, hoping rates of hole and electron carriers are inversely relying on the λ_h or λ_e whereas those are proportionally depending on t_h or t_e. The λ_h or λ_e can be generally derived from Nelson's four-point method by following equation[28].

$$IP = E_{cation} - E_{neutral} \tag{1}$$

$$EA = E_{neutral} - E_{anion} \tag{2}$$

$$\eta = \frac{(IP - EA)}{2} \tag{3}$$

$$\chi = \frac{(IP + EA)}{2} \tag{4}$$

$$\lambda_h = \left(\lambda^{cation}_{neutral} - \lambda_{cation}\right) + \left(\lambda^{neutral}_{cation} - \lambda_{neutral}\right) \tag{5}$$

$$\lambda_e = \left(\lambda^{anion}_{neutal} - \lambda_{anion}\right) + \left(\lambda^{neutral}_{anion} - \lambda_{neutral}\right) \tag{6}$$

Transfer integral implies the transfer probability of the electron and hole carriers between two neighboring molecules. This can be computed by a certain degree of wavefunction overlap between two adjacent molecules. Therefore, the non-covalently interacted dimer structures must be considered to gain the transfer integral of hole and electron (t_h and t_e). Unfortunately, the B3LYP functional lacks the non-covalent interaction parameter, hence it is inadequate to describe the non-covalent interaction. Accordingly, Grimme's dispersion correction with Bekes–Johnson damping (GD3BJ) was additionally utilized to describe the non-covalent interaction of pair structure[29]. The energy splitting by intermolecular polarization effect was further considered to obtain transfer integral. The t_h and t_e can be expressed by following equation[30].

$$t^{eff} = \frac{t_{12} - \frac{1}{2}(e_1 + e_2) S_{12}}{1 - S_{12}^2}, \tag{7}$$

where t_{12}, e_1, and e_2 are matrix elements for system Hamiltonian. S_{12} is the spatial electron density overlap integral between two the highest occupied molecular orbitals (HOMOs) or the LUMOs. The field-independent carrier hopping rates were derived by Marcus formalism as following Eq. (5).

$$k_{ET} = \frac{4\pi^2 t^2}{h}\sqrt{\frac{1}{4\pi\lambda k_B T}} exp\left(-\frac{(\lambda + \Delta G)^2}{4\lambda k_B T}\right), \tag{8}$$

where t, λ, k_B, h, T, and ΔG are defined as transfer integral, reorganization energy, Boltzmann constant, Plank constant, temperature, and Gibbs free energy, respectively.

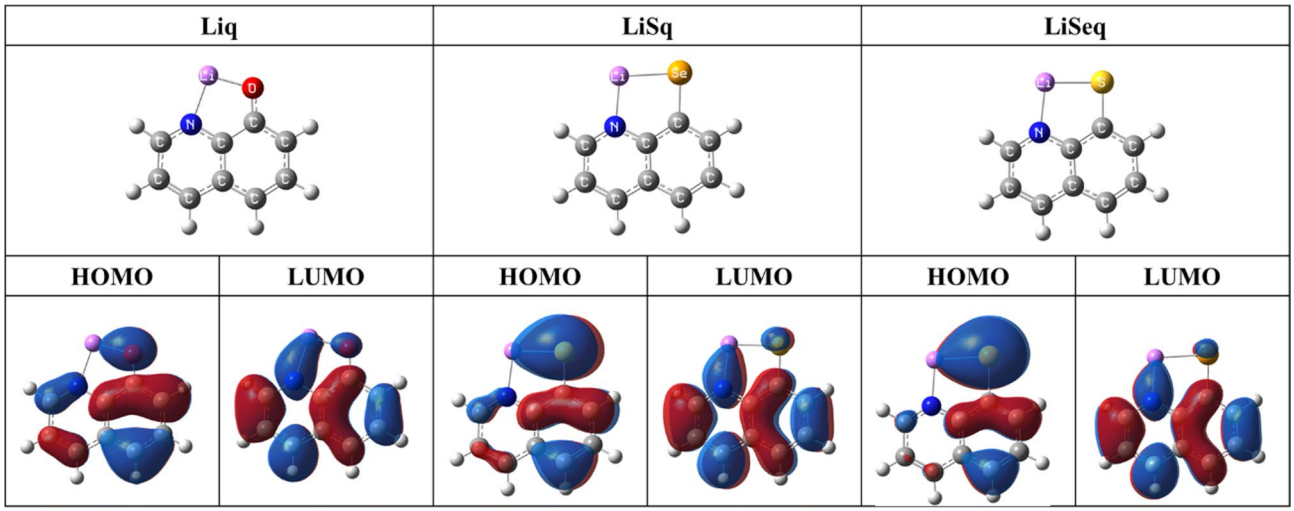

Fig. 1. The optimized molecular structure of MQ, MSQ, and MSeQ complexes.

	$d_{O/S/Se-M}$ (Å)	d_{N-M} (Å)	HOMO (eV)	LUMO (eV)	IP (eV)	EA (eV)	η (eV)	χ (eV)
Liq	1.752	1.962	-4.883	-1.527	6.567	0.086	3.240	3.326
LiSq	1.763	1.945	-4.905	-1.943	6.605	0.397	3.104	3.501
LiSeq	1.919	1.949	-4.762	-2.003	6.521	0.468	3.026	3.494

	λ_h (eV)	λ_e (eV)	t^2_h (eV)	t^2_e (eV)	k_h (s^{-1})	k_e (s^{-1})
Liq	0.345	0.090	0.034	0.067	3.410×10^{13}	1.050×10^{14}
LiSq	0.227	0.344	0.004	0.134	1.480×10^{13}	1.820×10^{13}
LiSeq	0.199	0.338	0.04	0.001	2.190×10^{14}	3.860×10^{8}

Table 1. The structural, electronic, and charge transport parameters of liq, lisq, and liseq.

The time dependent DFT (TDDFT) calculations were conducted to gain the absorption energies of these complexes.

Results and discussion

The role of S and Se atom in Li-based complex

To investigate the role of S and Se atoms on the electronic and charge transport property, we designed and optimized Liq, LiSq, and LiSeq. The optimized structures were depicted in Fig. 1. There are no remarkable changes in structural planarity. The structural parameters and electronic properties of Liq, LiSq, and LiSeq are listed in Table 1. Compared to Liq, the distances between S/Se and Li^+ are elongated, but the distance between N and Li^+ are slightly shortened. In the electronic properties, the highest occupied molecular orbital (HOMO) energy of LiSq is slightly shifted to deep level, but that of LiSeq is significantly shifted to shallow level. On the other hand, the energy level of the lowest unoccupied molecular orbital (LUMO) is gradually stabilized in the presence of the S and Se atoms. In terms of the electron injection, S and Se atoms play a beneficial role in minimizing the electron injection barrier between EIL and work-function of Al cathode ($\Phi = 4.2$ eV). This is due to the more stabilized LUMO energy level. Moreover, chemical hardness (η) of LiSq and LiSeq is smaller than that of Liq, indicating that the LiSq and LiSeq are relatively unstable during the redox reaction. In other words, introducing S and Se atoms may play a beneficial role in activating the oxidation and reduction process. As shown in Fig. 1, the spatial distributions of HOMO and LUMOs densely spread on the organic moiety in all complexes. However, it is noticed that LiSq and LiSeq show more localized electron density in HOMO. In OLED device, the mobility, which is known as decision factor for concentration of hole and electron carriers into EML, plays an important role in determining the *J-V* characteristic and power efficiency. According to the Einstein relation equation[31], the interrelationship between mobility and hopping rate is proportional. As we mentioned in the computational details, the hopping rate is proportional to the transfer integral and inversely proportional to the reorganization energy, according to the Marcus formalism. Comprehensively considering these relationships, it can be understood that hopping rate is one of important parameter to determine the OLED device performance. The computed parameters for charge transport property are listed in Table 2. The λ_h values of LiSq and LiSeq are tremendously decreased, but their λ_e values are significantly increased. This result indicates that the S and Se atoms play a beneficial role in suppressing the structural relaxation during the oxidation process. In contrast to this, these atoms are ineffective to reduce the structural relaxation during the reduction process. The t^2_h and t^2_h

	$d_{O/S\text{-}M}$ (Å)	$d_{N\text{-}M}$ (Å)	HOMO (eV)	LUMO (eV)	IP (eV)	EA (eV)	η (eV)	χ (eV)
NaSq	2.540	2.317	-4.601	-1.611	6.258	0.480	2.889	3.369
NaSeq	2.641	2.324	-4.501	-1.691	6.209	0.466	2.871	3.338
KSq	2.884	2.695	-4.312	-1.353	5.946	0.493	2.726	3.219
KSeq	3.001	2.699	-4.197	-1.431	5.885	0.481	2.702	3.183
RbSq	3.184	2.936	-4.035	-1.651	5.652	0.691	2.481	3.172
RbSeq	3.267	2.941	-3.947	-1.648	5.610	0.656	2.477	3.133
CsSq	3.393	3.142	-3.868	-1.601	5.485	0.678	2.404	3.081
CsSeq	3.483	3.142	-3.771	-1.607	5.432	0.655	2.389	3.043
AgSq	2.448	2.355	-5.122	-2.455	6.727	1.038	2.845	3.883
AgSeq	2.522	2.372	-5.027	-2.336	6.695	0.947	2.874	3.821
AuSq	2.347	2.540	-5.518	-3.062	7.086	1.594	2.746	4.340
AuSeq	2.426	2.585	-5.425	-2.944	7.045	1.480	2.782	4.262

Table 2. The structural and electronic parameters of a series of MSq and MSeq (M = Na, K, Rb, Cs, Ag, and Au).

values were computed from dimer structures. The t^2_h of LiSq is much smaller, but that of LiSeq is slightly larger than that of Liq. On the other hand, the t^2_e of LiSq is much larger, but that of LiSeq is tremendously.

smaller than that of Liq. To exactly compare the charge transport property, the hopping rates of hole and electron (k_h and k_e) were calculated. As a result, the computed k_h of LiSq is slightly decreased while that of LiSeq is 10-times faster than Liq. However, the calculated k_e values of LiSq and LiSeq are smaller than that of Liq. From these results, it is worthying noticed that introducing the S and Se atoms plays a beneficial role in lowering the electron injection barrier, whereas these atoms seem to be ineffective to improve the electron transport property. Nonetheless, the further investigation is necessary to clearly judge the role of S and Se atoms on charge transport property. This is because the strong perturbation effect of the different M^+ on the MO energy and charge transport property was previously reported.

M^+ (M = Na, K, Rb, Cs, Ag, and Au) effect

The optimized structures of MSq and MSeq complexes (M = Na, K, Rb, Cs, Ag, and Au) are denoted in Fig. 2. Similar to LiSq, and LiSeq, the structural planarity of a series of M^+Sq^- and M^+Seq^- complexes are sustained. Compared to Li-based complexes, $d_{S/Se-M}$ and d_{N-M} values are significantly increased due to the large van der Waals (vdW) radius.

Compared to Liq, the HOMO and LUMO energies of MSq and MSeq complexes (M = Na, K, Rb, and Cs) are shifted to deeper level, but these are more destabilized than those of LiSq and LiSeq. On the other hand, the HOMO and LUMO energies of MSq and MSeq complexes (M = Ag and Au) shifted to the deeper level, compared to Li-based complexes. This result implies the advantageous role of Ag^+ and Au^+ on the reduction of energy barrier between EIL and cathode.

The spatial distributions of HOMOs and LUMOs for all M^+Sq^- and M^+Seq^- (M = Na, K, Rb, Cs, Ag, and Au) are depicted in Fig. 2. For NaSq, NaSeq, and KSeq, HOMO and LUMO shapes are quite similar to LiSq and LiSeq. On the other hand, it is interested to notice that the spatial distribution of HOMO predominantly lies on the Sq/Seq moiety while that of LUMO mainly spreads on the metal ion in a series of MSq (M = K, Rb, Cs, Ag, and Au) and MSeq (M = Rb, Cs, Ag, and Au). Moreover, the contribution of S and Se atomic orbitals to both HOMO and LUMO is meaningfully increased in AgSq, AuSq, AgSeq, and AuSeq. From MO shapes, the transition characteristic can be assigned as ligand to metal charge transfer (LMCT). Similar to previous report[20] the metal ion plays a key determinant to change the MO shapes. As the change in M^+ ions, the calculated LUMO energies of MSq and MSeq (M = Na, Rb, Cs, Ag, and Au) are more stable than Liq. This result indicates that the most complexes are expected to reveal the superior electron injection property than Liq due to the decrease in the energy difference between work-function of Al-cathode and LUMO energy.

The computed λ, t, and hopping rate (k) of hole and electron carriers were summarized in Table 3. The calculated λ_h values of MSq and MSeq (M = Na, Ag, and Au) are smaller than that of LiSq and LiSeq, while those of MSq and MSeq (M = K, Rb, and Cs) are slightly larger than that of LiSq and LiSeq. On the other hand, the λ_e values of MSq and MSeq (M = Na, K, Rb, and Cs) are remarkably decremented, but those of MSq and MSeq (M = Ag and Au) are significantly increased, compared to those of LiSq and LiSeq. From these results, it is clearly understood that Ag and Au plays an advantageous role in suppressing the structural relaxation under the oxidation process. However, alkali metals (Na, K, Cs, and Se) efficiently suppress the structural relaxation under the reduction process. Nonetheless, λ_e values of all complexes are much larger than Liq. Let us turn to see the t^2_h and t^2_e. Compared to Li-based complexes, the computed t^2_h values are significantly incremented except NaSq NaSeq, RbSq, CsSq, and AgSq. In the case of t^2_e, NaSq, KSeq, RbSq, and CsSq are computed to be less unfavorable than LiSq. Considering the role of EIL materials, it is interested to mention that Ag^+ and Au^+ surprisingly activate the probability of the intermolecular electron transfer. To exactly compare the charge transport characteristic of these complexes, the derived k_h *and* k_e values are compared. The calculated k_h of Liq, LiSq and LiSeq are $3.41\times10^{13}\ s^{-1}$, $1.48\times10^{13}\ s^{-1}$ and $2.19\times10^{14}\ s^{-1}$, which are greatly increased in KSq, KSeq, CsSeq, AgSq, AgSeq, Auq, and AuSeq with the magnitude range of 10^{14}–$10^{17}\ s^{-1}$. For k_e, the derived rates

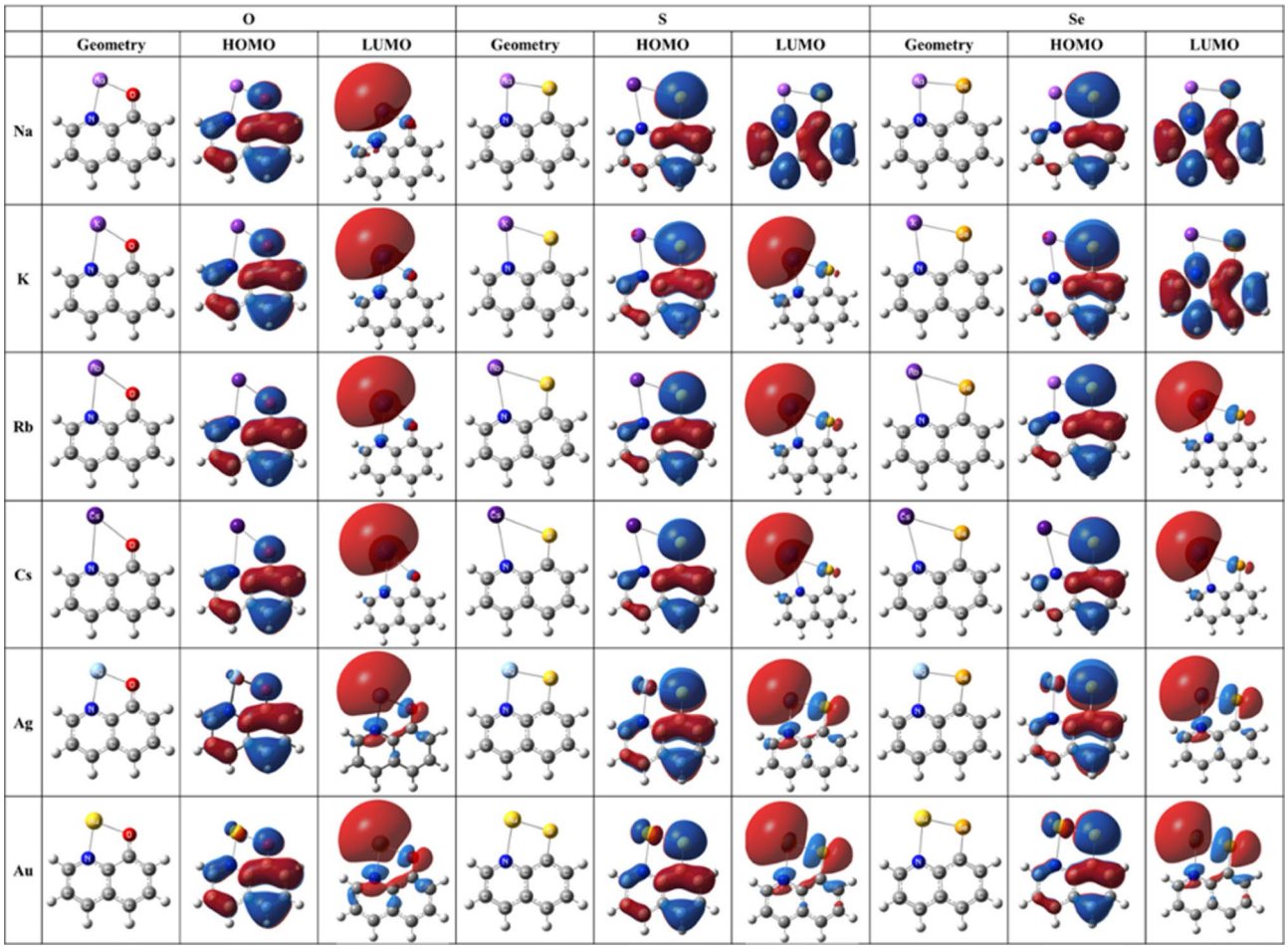

Fig. 2. The optimized molecular structure of MQ, MSQ, and MSeQ complexes.

	λ_h (eV)	λ_e (eV)	t^2_h (eV)	t^2_e (eV)	k_h (s^{-1})	k_e (s^{-1})
NaSq	0.218	0.167	$1.1*10^{-5}$	0.022	4.510×10^{10}	3.890×10^{12}
NaSeq	0.197	0.146	0.015	0.364	8.460×10^{13}	1.420×10^{15}
KSq	0.237	0.145	0.123	0.775	4.220×10^{14}	6.490×10^{15}
KSeq	0.214	0.130	4.461	0.012	2.020×10^{16}	2.010×10^{12}
RbSq	0.229	0.158	0.014	0.050	1.200×10^{13}	3.560×10^{13}
RbSeq	0.212	0.167	2.361	3.040	1.690×10^{16}	3.230×10^{16}
CsSq	0.239	0.139	0.007	0.085	2.320×10^{13}	8.440×10^{13}
CsSeq	0.221	0.148	2.964	4.265	1.230×10^{16}	1.880×10^{17}
AgSq	0.186	0.629	0.022	11.066	1.400×10^{14}	5.730×10^{15}
AgSeq	0.141	0.610	0.692	8.120	7.890×10^{15}	3.740×10^{15}
AuSq	0.182	0.772	0.071	13.497	4.740×10^{14}	1.900×10^{15}
AuSeq	0.144	0.727	9.572	146.827	1.040×10^{17}	3.590×10^{17}

Table 3. The charge transport parameters of MSq and MSeq (M = Na, K, Rb, Cs, Ag, and Au).

of MSq and MSeq (M = Na, K, Rb, Cs, Ag, and Au) are computed to be in the range of 10^{12}–10^{17} s^{-1}. Among them, MSq (M = K, Ag, and Au) and MSeq (M = Na, Rb, Cs, Ag, and Au) complexes are expected to be 10–100 times faster than Liq. Although the structural changes are inefficiently suppressed during the redox reaction, the intermolecular overlap of molecular orbitals helps to achieve the excellent hopping rates.

In other words, these results indicates that the most contributable parameter of charge transport is the transfer integral in these molecular systems. As already mentioned in the introduction, A key role of EIL material is to greatly increase the amount of injected electron from cathode and efficiently transfer the electron carrier into adjacent organic layer. Accordingly, the small injection barrier and good electron transport properties are

essentially required to deliver a large amount of electron carriers into the EML, leading to the enhancement of exciton recombination. From the comprehensive consideration of LUMO energy and k_e results, it is expected that Ag and Au ions binding with Sq and Seq moiety play an advantageous role in reducing the energy barrier and enhancing the k_e.

Absorption property

In the top emitting device, the light is extracted through the cathode. To maximize the efficiency of the top-emitting device, three primary color lights must be entirely extracted without any loss of photon by absorption of ET-side layers. With this perspective, the absorption property of EIL should be carefully considered as one of parameter to effect on the device efficiency. Prior to compute the absorption energy, the adequate DFT functional should be chosen to accurately predict the absorption energy. Accordingly, B3LYP[23–25] CAM-B3LYP[32]ωB97xD[33] and LC-ωHPBE[34–36] functionals with 6-311G** basis set were examined to compare the absorption energy of Liq in experiment. As a result, the computed absorption energies of Liq by different DFT functionals are 2.799 eV (B3LYP), 3.256 eV (CAM-B3LYP), 3.290 eV (ωB97xD), and 3.642 eV (LC-ωHPBE), respectively, which correspond to the absorption wavelengths of 443.02, 380.84, 376.90, and 340.47 nm, respectively. In the experiment, the absorption wavelength of Liq was measured at 365 nm, which is in good agreement with the result of the ωB97xD calculation.

Therefore, the absorption energies of all designed complexes were computed by TD-ωB97xD/6-311G** level of theory and the corresponding values are listed in Table 4. The absorption energies of all complexes are shifted to lower energy than Liq. Given the emission wavelengths of primary colors in commercial OLED devices (blue = 455 nm, green = 530 nm, red = 630 nm), the most of complexes are expected not to remarkably influence on the efficiency drop of top-emitting OLED devices except CsSeq, AgSq, AgSeq, AuSq, and AuSeq. It is important to note that CsSeq, AgSq, AgSeq, AuSq, and AuSeq may very minorly impact on the efficiency drop of the blue emission due to the slight overlap of the absorption and emission wavelengths. Specifically, the blue absorption of CsSq, AgSq, and AgSeq is originated from the 1st excited state, while that of AuSq and AuSeq occurs in the 2nd excited state. (See Fig. S2) Nonetheless, the computed oscillator strengths of all designed molecules are too small to abundantly absorb the photons. This result indicates that a series of MSq and MSeq complexes may hardly impact on the efficiency drop in OLED devices.

Complexation with ETL

Previously, we reported the complexation effect of Liq with electron transport material (ETM) on the charge transport property[37] which critically reduces k_h and k_e due to increase in λ and decrease in t^2.With this perspective, the complexation effect of newly designed EIL complexes with ETM on the charge transport property was investigated. The most popular core skeleton for ETM is triazine moiety since the strong electron acceptability and structural planarity are beneficial to efficiently transport the electron carrier. Therefore, 2,4,6-tris(biphenyl-3yl)-1,3,5-triazine (T2T) was selected as the representative ETL material in this study. For triazine-based ETM, the root cause of the complexation effect on the small t^2 can be understood that planar structure of triazine core can be broken since the intramolecular H-bonds defined as C-H…N H-bond are dismantled by coordination bond between N and M^+. Accordingly, the bulkiness of ETL material is increased, thereby the inefficient intermolecular interactions enable the reduction of the molecular orbital overlap. In addition, the coordinated EIL material induces the shielding effect to interrupt the effective overlap of the molecular orbitals. Therefore, we solely computed λ_h and λ_e of coordinated structures between individual designed EIL material and T2T. These values are listed in Table 5 and their $\Delta\lambda$ ($\lambda_{T2T-MXq\ (X=\ S\ and\ Se)}$ - $\lambda_{T2T-Liq}$) values are depicted in Fig. 3. In addition, the optimized structures were denoted in Fig S1.

	Absorption energy (eV)	Absorption energy (nm)	Oscillator strength (*f*)
Liq	3.290	376.90	0.0651
LiSq	3.081	402.47	0.1037
LiSeq	2.949	420.48	0.0934
NaSq	3.112	398.46	0.1295
NaSeq	2.996	413.89	0.1204
KSq	3.090	401.29	0.1361
KSeq	2.956	419.49	0.1272
RbSq	2.986	415.27	0.0121
RbSeq	2.836	437.24	0.0167
CsSq	2.950	420.34	0.0111
CsSeq	2.785	445.24	0.0161
AgSq	2.754	450.25	0.0101
AgSeq	2.691	460.80	0.012
AuSq	2.221	558.31 (474.48)	0.0062 (0.0281)
AuSeq	2.168	571.96 (462.71)	0.0068 (0.0387)

Table 4. The calculated absorption energy and oscillator strength. The absorption wavelengths and oscillator strengths for 2nd excited state are listed in parentheses.

	λ_h (eV)	λ_e (eV)
T2T	0.128	0.269
T2T-Liq	0.498	0.374
T2T-LiSq	0.488	0.373
T2T-LiSeq	0.319	0.374
T2T-NaSq	0.398	0.393
T2T-NaSeq	0.307	0.354
T2T-KSq	0.336	0.424
T2T-KSeq	0.311	0.327
T2T-RbSq	0.361	0.421
T2T-RbSeq	0.343	0.394
T2T-CsSq	0.358	0.424
T2T-CsSeq	0.353	0.415
T2T-AgSq	0.310	0.382
T2T-AgSeq	0.280	0.372
T2T-AuSq	0.279	0.369
T2T-AuSeq	0.282	0.369

Table 5. The computed λ_h*and* λ_e of T2T-MSq and T2T-MSeq complexes.

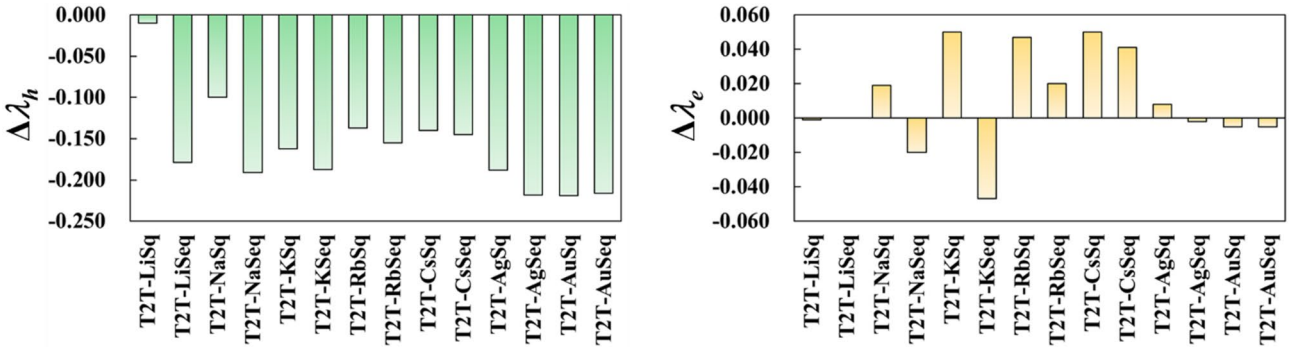

Fig. 3. The chart graph for difference between $\lambda_{T2T-MXq\ (X=\ S\ and\ Se)}$ and $\lambda_{T2T-Liq}$.

Compared to both λ of T2T, the complexation between T2T and MSq/MSeq clearly impacts to the increment of λ_h and λ_e. As shown in Fig. 3, the λ_h values of T2T-MSq and T2T-MSeq (M = Li, Na, K, Rb, Cs, Ag, and Au) complexes are decremented, compared to T2T-Liq complex. In addition, the λ_e values of T2T-NaSeq, T2T-KSeq, T2T-AgSeq, T2T-AuSq, and T2T-AuSeq are slightly decreased while those of T2T-NaSq, T2T-KSq, T2T-RbSq, T2T-RbSeq, T2T-CsSq, T2T-CsSeq, and T2T-AgSq are slightly increased. As aforementioned, Liq is co-deposited with ETM to form ETL, resulting in the presence of the undesired complex between Liq and ETM. Therefore, forming a complex between ETM and EIL interrupts the spontaneous electron transfer between adjacent molecules, reducing the amount of electron carriers into EML. With this perspective, NaSeq, KSeq, AgSeq, AuSq, and AuSeq are expected to slightly mitigate the weakening the electron transport property under the complexation with ETM.

For commercial OLED device, the demands for highly efficient OLED device with excellent power efficiency have been gradually increased. With this perspective, it is expected that AuSq and AuSeq play a pivotal role in improving the efficiency and the power efficiency since the fast electron transport property and small injection barrier of these materials decrease the turn-on voltage and increase the electron carrier concentration. Moreover, these materials are expected to slightly weaken the electron transport property under the complexation with ETL material. Accordingly, we propose AuSq and AuSeq as candidate EIL material to replace the current Liq for achieving the highly efficient OLED device.

Conclusion

In this study, the candidate EIL materials, which can be used as alternative materials of Liq, were designed and investigated with DFT computation. Based on the quinolate skeleton, the S and Se atoms were utilized to replace the O in the quinolate moiety. In addition, the effect of introducing the different singly oxidized metal ions was also considered. As increase the demand for high power efficiency of OLED device, the electron transport and electron injection properties play an important role in enhancing these performances since the *J-V* characteristic of OLED device strongly depends on the electron transport. Therefore, the development of charge transport property for EIL is essentially required to further improve the power efficiency. From this perspective, with Li^+

ion, the effect of introducing S and Se atoms on the electron transport property is diadvantageous. However, the electron transport property is significantly enhanced with different M ions except NaSq, KSeq, RbSq, and CsSq. In the point of view for the side effect of EIL material on the performance of OLED device, the absorption energies of designed EIL materials and $\lambda_{h/e}$ of ETM-MSq/MSeq complexes were additionally considered. Except CsSeq, AgSq, and AgSeq, the effect of the absorption energies on the device performance can be negligible in all designed materials. In addition to this, NaSeq, KSeq, AgSeq, AuSq, and AuSeq are beneficial to weaken the increase of λ_e via forming a complex with ETM. From comprehensive analysis of our theoretical results, we suggest that the utilization of AuSq or AuSeq as EIL is expected to reveal the superior device performance, compared to conventional Liq.

Data availability

The authors declare that most data supporting this study are included in this article. The rest of the data generated and/or analyzed during this study are available from the corresponding authors on the reasonable request.

Received: 27 April 2025; Accepted: 30 June 2025
Published online: 06 July 2025

5. References

1. Tang, C. W. & VanSlyke, S. A. Organic electroluminescent diodes. *Appl. Phys. Lett.* **51**, 913–915 (1987).
2. Rogers, J. A., Someya, T. & Huang, Y. Materials and mechanics for stretchable electronics. *Science* **327**, 1603–1607 (2010).
3. Kim, S. et al. Low-power flexible organic light-emitting diode display device. *Adv. Mater.* **23**, 3511–3516 (2011).
4. Geffroy, B., Le Roy, P. & Prat, C. Organic light-emitting diode (OLED) technology: materials, devices and display technologies. *Polym. Int.* **55**, 572–582 (2006).
5. Salehi, A., Fu, X., Shin, D. H. & So, F. Recent advances in OLED optical design. *Adv. Funct. Mater.* **29**, 1808803 (2019).
6. Sun, J. et al. Exceptionally stable blue phosphorescent organic light-emitting diodes. *Nat. Photonics*. **16**, 212–218 (2022).
7. Zhang, Q. et al. Efficient blue organic light-emitting diodes employing thermally activated delayed fluorescence. *Nat. Photonics*. **8**, 326–332 (2014).
8. Li, W. et al. A hybridized local and charge-transfer excited state for highly efficient fluorescent oleds: molecular design, spectral character, and full exciton utilization. *Adv. Opt. Mater.* **2**, 892–901 (2014).
9. Hong, G. et al. A brief history of OLEDs—emitter development and industry milestones. *Adv. Mater.* **33**, 2005630 (2021).
10. Tsang, D. P. K., Matsushima, T. & Adachi, C. Operational stability enhancement in organic light-emitting diodes with ultrathin liq interlayers. *Sci. Rep.* **6**, 22463 (2016).
11. Zhao, H., Arneson, C. E., Fan, D. & Forrest, S. R. Stable blue phosphorescent organic leds that use polariton-enhanced Purcell effects. *Nature* **626**, 300–305 (2024).
12. Zhang, Y., Lee, J. & Forrest, S. R. Tenfold increase in the lifetime of blue phosphorescent organic light-emitting diodes. *Nat. Commun.* **5**, 5008 (2014).
13. Heimel, P. et al. Unicolored phosphor-sensitized fluorescence for efficient and stable blue OLEDs. *Nat. Commun.* **9**, 4990 (2018).
14. Kim, K. J., Lee, H., Kang, S. & Kim, T. Superbly long lifetime over 13,000 h for multiple energy transfer channels in deep blue phosphorescence organic light-emitting diodes with Ir complex under CIEy of 0.17. *Chem. Eng. J.* **448**, 137671 (2022).
15. Lee, H. et al. Superbly efficient and stable ultrapure blue phosphorescent organic Light-Emitting diodes with tetradentate Pt (II) complex with vibration suppression effect. *Adv. Mater.* **36**, 2409394 (2024).
16. Wong, B. Y. W., Wong, H. L., Wong, Y. C., Chan, M. Y. & Yam, V. W. W. Versatile synthesis of luminescent tetradentate cyclometalated Alkynylgold (III) complexes and their application in Solution-Processable organic Light-Emitting devices. *Angew. Chem.* **129**, 308–311 (2017).
17. Aizawa, N. et al. Delayed fluorescence from inverted singlet and triplet excited States. *Nature* **609**, 502–506 (2022).
18. Schmitz, C., Schmidt, H. W. & Thelakkat, M. Lithium – quinolate complexes as emitter and interface materials in organic light-emitting diodes. *Chem. Mater.* **12**, 3012–3019 (2000).
19. Kang, S. & Kim, T. The nature of electronic and carrier transport properties of M-(quinolate) 2 complexes (M = Be, mg, ca, and Sr): A computational study. *Org. Electron.* **87**, 105980 (2020).
20. Jeon, S. H., Cho, Y. M., Kim, T. & Kang, S. Discovering new M-quinolate materials: theoretical insight into Understanding the charge transport, electronic, self-aggregation properties in M-quinolate materials (M = Li, na, K, rb, cs, cu, ag, and Au). *J. Mater. Sci.* **54**, 9523–9532 (2019).
21. Rajeswaran, M., Begley, W. J., Olson, L. P. & Huo, S. Steric effects of substituted Quinolines on lithium coordination geometry. *Polyhedron* **26**, 3653–3660 (2007).
22. Fang, X. H. et al. The effect of the cyano-group substitution on the electronic properties of 8-hydroxyquinoline lithium studied with DFT. *J. Mol. Struct. (Thoechem)*. **848**, 82–86 (2008).
23. Becke, A. D. Density-functional exchange-energy approximation with correct asymptotic behavior. *Phys. Rev. A*. **38**, 3098 (1988).
24. Lee, C., Yang, W. & Parr, R. G. Development of the Colle-Salvetti correlation-energy formula into a functional of the electron density. *Phys. Rev. B*. **37**, 785 (1988).
25. Becke, A. D. A new inhomogeneity parameter in density-functional theory. *J. Chem. Phys.* **109**, 2092–2098 (1998).
26. Frisch, M. et al. (Gaussian, Inc. 2016).
27. Marcus, R. A. *In Protein electron Transfer* 249–272 (Garland Science, 2020).
28. Nelsen, S. F., Blackstock, S. C. & Kim, Y. Estimation of inner shell Marcus terms for amino nitrogen compounds by molecular orbital calculations. *J. Am. Chem. Soc.* **109**, 677–682 (1987).
29. Grimme, S., Ehrlich, S. & Goerigk, L. Effect of the damping function in dispersion corrected density functional theory. *J. Comput. Chem.* **32**, 1456–1465 (2011).
30. Kang, S., Moon, J. H., Kim, T. & Lee, J. Y. Design of efficient non-doped blue emitters: toward the improvement of charge transport. *RSC Adv.* **9**, 27807–27816 (2019).
31. Liu, H., Kang, S. & Lee, J. Y. Electronic structures and charge transport of stacked annelated β-trithiophenes. *J. Phys. Chem. B*. **115**, 5113–5120 (2011).
32. Yanai, T., Tew, D. P. & Handy, N. C. A new hybrid exchange–correlation functional using the Coulomb-attenuating method (CAM-B3LYP). *Chem. Phys. Lett.* **393**, 51–57 (2004).
33. Chai, J. D. & Head-Gordon, M. Long-range corrected hybrid density functionals with damped atom–atom dispersion corrections. *Phys. Chem. Chem. Phys.* **10**, 6615–6620 (2008).
34. Vydrov, O. A. & Scuseria, G. E. Assessment of a long-range corrected hybrid functional. *J. Chem. Physics* 125 (2006).
35. Vydrov, O. A., Heyd, J., Krukau, A. V. & Scuseria, G. E. Importance of short-range versus long-range Hartree-Fock exchange for the performance of hybrid density functionals. *J. Chem. Physics* 125 (2006).

36. Vydrov, O. A., Scuseria, G. E. & Perdew, J. P. Tests of functionals for systems with fractional electron number. *J. Chem. Phys.* 126 (2007).
37. Kang, S., Jeon, S. H. & Kim, T. Unraveling the complexation effect of electron transporting materials with liq on the charge transport properties: A theoretical perspective. *Chem. Phys. Lett.* **810**, 140207 (2023).

Acknowledgements
This work was supported by the Ministry of Trade, Industry, and Energy of the Republic of Korea (RS-2024-00419747 and RS-2024- 00418716).

Author contributions
Sunwoo Kang: Writing – review & editing, Writing – original draft, Supervision, Methodology, Investigation, Funding acquisition, Formal analysis, Data curation, Conceptualization. Taekyung Kim: Writing –review & editing, Supervision, Formal analysis, Conceptualization.

Declarations

Competing interests
The authors declare no competing interests.

Additional information
Supplementary Information The online version contains supplementary material available at https://doi.org/10.1038/s41598-025-09721-5.

Correspondence and requests for materials should be addressed to S.K. or T.K.